JOURNAL OF SOLID STATE CHEMISTRY **131,** 335–340 (1997)
ARTICLE NO. SC977389

# Magnetic Behavior of $Na_2MSi_4O_{10}$ ($M$ = Co, Ni) Compounds

G. Durand, S. Vilminot,[1] M. Richard-Plouet, A. Derory, J. P. Lambour, and M. Drillon

*Groupe des Matériaux Inorganiques, IPCMS, UMR 46 CNRS, 23 rue du Loess, 67037 Strasbourg Cedex, France*

Received November 12, 1996; in revised form March 4, 1997; accepted March 11, 1997

**$Na_2MSi_4O_{10}$ ($M$ = Co, Ni) compounds have been obtained by annealing at 700°C a xerogel prepared from silicon and sodium ethoxides and $M$ nitrate. Both silicates appear to be isostructural with the corresponding copper phase, with the presence of silicate pipes built up from $(Si_8O_{20})^{8-}$ units. The $M$ cations define isolated $(M_2O_8)^{4-}$ dimers from two edge-sharing square pyramids with $M$–$M$ distances of around 3.17 Å. The magnetic properties have been analyzed as the presence of ferromagnetic interactions inside the dimers and antiferromagnetic interactions between the dimers at low temperature.** 

## INTRODUCTION

Consideration of silicate compounds reveal a great complexity of the $SiO_4$ building blocks with many possibilities: isolated tetrahedra, chains, double chains, cycles, layers, etc. The same variety of structural units also appear in the corresponding cationic network, which can be a source for various magnetic behavior if transition metals are involved. In a previous paper (1), we considered the synthesis and structural and magnetic properties of pyroxene-like compounds, $CaMSi_2O_6$ ($M$ = Co, Ni), exhibiting infinite $MO_6$ chains. The presence of copper isolated dimers has been shown in the structure of $Na_2CuSi_4O_{10}$ (2). We therefore considered the possibility of preparing the corresponding cobalt and nickel compounds to relate structural data with magnetic properties.

## EXPERIMENTAL

Both samples were prepared starting from sodium ($NaOC_2H_5$) and silicon ($Si(OC_2H_5)_4$, TEOS) ethoxides and transition metal nitrate as precursors. Two alcoholic solutions were prepared, the first containing sodium, and the second containing Si, $M$, and $H_2O$ to promote TEOS prehydrolysis. After both solutions were mixed, gelation took place immediately. The resulting samples were air dried at 40°C to remove most of the solvent and then calcined at 300°C to decompose the nitrates.

The samples were annealed at different temperatures ranging from 400 to 750°C and subsequently identified by X-ray diffraction. Whereas the samples remained amorphous up to 500°C, crystallization started at around 600°C and pure phases were obtained after 10 h at 700°C. For annealing experiments at temperature higher than 700°C, melting was observed.

The following techniques were used to characterize the samples: thermogravimetric (TGA) and differential thermal (DTA) analysis on a TGA92 Setaram apparatus, X-ray diffraction on a Siemens D500 powder diffactometer using monochromatized Co$K\alpha_1$ radiation, Rietveld powder refinements using the Fullprof program (3), magnetic susceptibility on a Manics Faraday-based magnetosusceptometer, and specific heat using a quasi-adiabatic method (4).

## RESULTS AND DISCUSSION

### *Thermal Evolution*

Thermal evolution is quite similar for both compounds. As shown in Fig. 1 in the case of $Na_2NiSi_4O_{10}$ previously dried at 120°C, the weight loss proceeds within three steps. The first step, at low temperature (20–100°C), is associated with a strong endothermal effect and could be related to the evaporation of adsorbed species. The second step, between around 300 and 600°C, is associated with two endothermal effects (only one for the Co compound). The third step appears between around 700 and 775°C (shifted by 40°C toward lower temperature for Co). A small and broad endothermal effect appears in the same temperature domain. Therefore, any exothermal effect that could be related to crystallization does not appear on the DTA trace.

Assuming that the weight loss below 100°C is related to adsorbed species, the following explanation is proposed for the weight loss observed above 100°C. In the presence of water, sodium alkoxide is transformed into NaOH. This compound promotes the condensation of previously prehydrolyzed TEOS, explaining why immediate gelation is observed. Further drying at 40°C yields the formation of

[1] To whom correspondence should be addressed.



0022-4596/97 $25.00

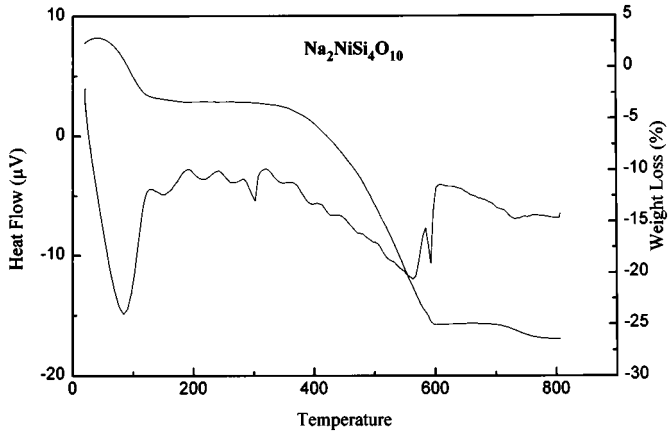


**FIG. 1.** TG-DTA traces of $Na_2NiSi_4O_{10}$ under air atmosphere using a 6°C/min heating rate.

amorphous silica. Moreover, NaOH also reacts with metal nitrate with formation of metal hydroxyde. The reaction scheme could be summarized

$$2NaOR + M(NO_3)_2 \cdot 6H_2O + 4Si(OC_2H_5)_4 + 16H_2O \downarrow \quad [1]$$

$$2NaOH + M(NO_3)_2 \cdot 6H_2O + 4Si(OH)_4 + 2ROH + 16\ C_2H_5OH \downarrow \quad [2]$$

$$2NaNO_3 + M(OH)_2 + 4SiO_2\ (\text{after } 100^\circ C \text{ drying}) \downarrow \quad [3]$$

$$Na_2MSi_4O_{10} + 2HNO_3.$$

The first two reactions do not take place one after each other as mentioned but are involved during the first step up to gel drying. Under these conditions, the expected weight loss during reaction [3] is around 25 wt%, compared to an observed value of around 23 wt%.

### *X-Ray Diffraction and Structure Refinement*

Samples previously dried at 300°C have been calcined at different temperatures and characterized by powder X-ray diffraction. After 500°C annealing, the samples remain X-ray amorphous. For higher annealing temperatures, 600, 650, and 700°C, the crystallinity is strongly time dependent. At the lowest temperatures, 600 and 650°C, after 72 and 24 h, respectively, a mixture containing *M* oxide and $Na_2MSi_4O_{10}$ is detected with three extra lines that have not been assigned. Pure $Na_2MSi_4O_{10}$ phases are observed after annealing for 10 h at 700°C. Attempts to prepare the corresponding copper phase under the same experimental conditions did not succeed, yielding a mixture of $Na_2CuSi_4O_{10}$, CuO, and silica even after numerous calcinations. The different reactivity of the copper system can explain why a pure phase is obtained only under hydrothermal conditions (2, 5).

As expected, Co and Ni compounds are isostructural with the corresponding copper phase (6) and their powder diffraction pattern can be indexed in a triclinic unit cell (Table 1). Structure refinements have been performed from powder X-ray diffraction data starting from the results of Kawamura and Kawahara (2). Table 1 gives the refinement conditions, Table 2 the final parameters, and Table 3 some interatomic distances.

The structure is made up of silicate pipes, exhibiting $(Si_8O_{20})^{8-}$ radicals as the report unit as shown in Fig. 2 drawn using the same unit cell transformation as Kawamura and Kawahara (2) to get a structure similar to litidionite, $CuNaKSi_4O_{10}$. Such radicals are connected to each other in the *c* axis direction (pipe axis) by oxygen atoms. In the *b*′ axis direction, the $SiO_4$ tetrahedra from two adjacent radicals do not share oxygen atoms and the cohesion of the structure is realized by means of Na(1) polyhedra with four intraradical and two interradical Na–O bonds, Na(1) atoms being inside the $(Si_8O_{20})^{8-}$ units whereas *M* and Na(2) are outside. In the *a*′ axis direction, the silicate pipes are linked by *M* and Na(2) polyhedra.

Both Na atoms have an irregular environment with seven oxygen neighbors. However, in the case of Na(2), the Na(2)–O(7) distance, 3.21 and 3.09 Å for Co and Ni, respectively, is significantly greater than the others. Similar results were observed for Na atoms in $Na_2CuSi_4O_{10}$ (2) (Table 4), with a Na(2)–O(7) distance of 3.047 Å.

**TABLE 1**
**Refinement Conditions (X-Ray Powder Data) for $Na_2MSi_4O_{10}$ Samples**

| | Co | Ni | | Co | Ni |
|---|---|---|---|---|---|
| *a*(Å) | 10.7173(6) | 10.6512(4) | α(°) | 117.394(3) | 117.849(3) |
| *b*(Å) | 7.8782(5) | 7.8295(3) | β(°) | 116.842(4) | 116.706(3) |
| *c*(Å) | 6.9402(4) | 6.9454(3) | γ(°) | 93.561(4) | 93.214(3) |
| *V*(Å$^3$) | 436.456 | 430.768 | *Z* | 2 | 2 |

| | Co | Ni |
|---|---|---|
| Space Group | *P*1 | *P*1 |
| 2θ range | 10–110 | 10–110 |
| Step scan °2θ | 0.02 | 0.02 |
| Reflection number | 570 | 685 |
| Profile parameter number | 12 | 12 |
| Atom number | 17 | 17 |
| $R_F$ (%) | 3.6 | 6.0 |
| $R_B$ (%) | 5.3 | 8.7 |
| $R_p$ (%) | 13.8 | 15.7 |
| $R_{wp}$ (%) | 18.0 | 21.6 |
| GoF (%) | 2.6 | 6.6 |

**TABLE 2**
**Refined Structural Parameters for $Na_2MSi_4O_{10}$ Compounds**

| | $x/a$ | $y/b$ | $z/c$ | $B$(Å$^2$) |
|---|---|---|---|---|
| Co | 0.4198(7) | 0.306(1) | 0.478(1) | 1.1(2) |
| Na(1) | 0.016 (1) | 0.238(2) | 0.905(2) | 2.0(3) |
| Na(2) | 0.422 (1) | 0.272(2) | 0.953(2) | 2.0(3) |
| Si(1) | 0.804 (1) | 0.072(2) | 0.113(2) | 1.9(3) |
| Si(2) | 0.138 (1) | 0.283(2) | 0.510(2) | 2.7(3) |
| Si(3) | 0.738 (1) | 0.365(2) | 0.494(2) | 3.3(4) |
| Si(4) | 0.751 (1) | 0.381(2) | 0.943(2) | 2.9(4) |
| O(1) | 0.976 (3) | 0.090(3) | 0.293(5) | 5.8(9) |
| O(2) | 0.736 (2) | 0.151(3) | 0.276(4) | 2.9(7) |
| O(3) | 0.280 (2) | 0.157(3) | 0.104(4) | 1.1(6) |
| O(4) | 0.273 (2) | 0.214(3) | 0.551(4) | 1.4(6) |
| O(5) | 0.585 (2) | 0.415(3) | 0.431(4) | 2.2(6) |
| O(6) | 0.578 (3) | 0.356(3) | 0.824(4) | 3.0(8) |
| O(7) | 0.128 (2) | 0.396(3) | 0.786(4) | 1.5(6) |
| O(8) | 0.807 (2) | 0.352(3) | 0.745(4) | 1.0(6) |
| O(9) | 0.128 (2) | 0.450(3) | 0.435(4) | 0.7(6) |
| O(10) | 0.797 (3) | 0.208(4) | 0.994(5) | 5.8(8) |
| Ni | 0.4241(5) | 0.3066(8) | 0.479(1) | 1.7(2) |
| Na(1) | 0.017 (1) | 0.237 (2) | 0.904(2) | 2.0(2) |
| Na(2) | 0.415 (1) | 0.263 (2) | 0.930(2) | 2.0(3) |
| Si(1) | 0.806 (1) | 0.059 (1) | 0.112(2) | 1.8(3) |
| Si(2) | 0.146 (1) | 0.297 (2) | 0.512(2) | 2.5(3) |
| Si(3) | 0.735 (1) | 0.362 (1) | 0.501(2) | 2.0(3) |
| Si(4) | 0.750 (1) | 0.375 (2) | 0.942(2) | 3.0(3) |
| O(1) | 0.994 (2) | 0.112 (3) | 0.320(4) | 5.6(7) |
| O(2) | 0.727 (2) | 0.155 (3) | 0.266(3) | 2.9(6) |
| O(3) | 0.263 (2) | 0.172 (2) | 0.093(3) | 0.6(4) |
| O(4) | 0.269 (2) | 0.203 (2) | 0.526(3) | 4.3(6) |
| O(5) | 0.580 (2) | 0.390 (2) | 0.406(3) | 1.3(5) |
| O(6) | 0.580 (2) | 0.366 (2) | 0.835(3) | 3.8(7) |
| O(7) | 0.144 (2) | 0.414 (3) | 0.797(4) | 3.8(6) |
| O(8) | 0.805 (2) | 0.367 (2) | 0.757(3) | 1.3(6) |
| O(9) | 0.124 (2) | 0.463 (3) | 0.429(3) | 5.0(6) |
| O(10) | 0.790 (2) | 0.198 (2) | 0.997(3) | 0.8(4) |

**TABLE 3**
**Interatomic Distances (Å)**

*M* polyhedron

| | Co | Ni |
|---|---|---|
| $M$–O(3) | 1.96(2) | 2.06(2) |
| $M$–O(5) | 2.00(3) | 2.09(2) |
| $M$–O(6) | 2.03(2) | 2.06(2) |
| $M$–O(4) | 2.04(3) | 2.02(2) |
| $M$–O(5) | 2.14(3) | 2.14(2) |
| ⟨$M$–O⟩ | 2.03 | 2.07 |

Na polyhedra

| | Co | Ni | | Co | NI |
|---|---|---|---|---|---|
| Na(1)–O(7) | 2.31(3) | 2.44(3) | Na(2)–O(4) | 2.29(2) | 2.30(2) |
| Na(1)–O(1) | 2.33(4) | 2.39(3) | Na(2)–O(6) | 2.41(3) | 2.36(3) |
| Na(1)–O(8) | 2.45(3) | 2.51(2) | Na(2)–O(3) | 2.52(3) | 2.59(2) |
| Na(1)–O(10) | 2.71(4) | 2.81(3) | Na(2)–O(6) | 2.60(3) | 2.56(3) |
| Na(1)–O(8) | 2.79(3) | 2.69(2) | Na(2)–O(2) | 2.92(3) | 2.88(3) |
| Na(1)–O(3) | 2.80(3) | 2.57(2) | Na(2)–O(5) | 2.53(2) | 2.55(2) |
| Na(1)–O(9) | 2.81(2) | 2.78(2) | Na(2)–O(7) | 3.21(3) | 3.09(3) |
| ⟨Na(1)–O⟩ | 2.6 | 2.60 | ⟨Na(2)–O⟩ | 2.55 | 2.62 |

Si tetrahedra

| | Co | Ni | | Co | Ni |
|---|---|---|---|---|---|
| Si(1)–O(2) | 1.54(3) | 1.60(2) | Si(2)–O(4) | 1.53(3) | 1.53(3) |
| Si(1)–O(3) | 1.55(3) | 1.52(2) | Si(2)–O(9) | 1.61(3) | 1.63(3) |
| Si(1)–O(10) | 1.61(4) | 1.60(2) | Si(2)–O(1) | 1.68(3) | 1.57(3) |
| Si(1)–O(1) | 1.64(4) | 1.73(3) | Si(2)–O(7) | 1.76(2) | 1.76(2) |
| ⟨Si(1)–O⟩ | 1.59 | 1.61 | ⟨Si(2)–O⟩ | 1.65 | 1.62 |
| Si(3)–O(8) | 1.61(2) | 1.57(2) | Si(4)–O(6) | 1.61(3) | 1.60(3) |
| Si(3)–O(5) | 1.62(3) | 1.55(2) | Si(4)–O(10) | 1.61(4) | 1.63(3) |
| Si(3)–O(2) | 1.66(3) | 1.64(2) | Si(4)–O(7) | 1.67(2) | 1.56(2) |
| Si(3)–O(9) | 1.69(3) | 1.69(3) | Si(4)–O(8) | 1.67(3) | 1.61(2) |
| ⟨Si(3)–O⟩ | 1.65 | 1.61 | ⟨Si(4)–O⟩ | 1.64 | 1.60 |

The main difference with the copper sample concerns the $M$ environment. Whereas copper has four nearest neighbors in the form of a square and one additional oxygen atom at a much longer distance (Table 4), the environment around Co and Ni looks like a more regular square pyramid. As shown in Fig. 3, two edge-sharing square pyramids around $M$ atoms define isolated $(M_2O_8)^{4-}$ dimers with $M$–$M$ distances around 3.17 Å.

*Magnetic Measurements*

The magnetic susceptibility of $Na_2NiSi_4O_{10}$ (Fig. 4), recorded at 12,800 Oe down to 50 K and at 600 Oe below, follows a Curie–Weiss law (Fig. 5) for temperatures ranging between 100 and 300 K, with a $\theta$ value characteristic of ferromagnetic behavior. The slight increase of the $\chi T$ product upon cooling down to 35 K (Fig. 6) confirms the presence of predominant ferromagnetic interactions, while at lower temperature the $\chi T$ variation indicates that the long-range ordering between Ni(II) ions is antiferromagnetic.

Similar behavior is observed for $Na_2CoSi_4O_{10}$ showing Curie–Weiss behavior in the range 300–150 K, in agreement with dominant ferromagnetic interactions (Fig. 5). In fact, the temperature dependence of $\chi T$ (Fig. 6) slightly differs due to the spin–orbit coupling effect for the Co(II) ion. A minimum of $\chi T$ is observed at around 30 K, then a slight increase up to 2.75 emu K/mol at 10.8 K, and a drop below 10 K related to antiferromagnetic couplings between Co(II) pairs. Table 5 summarizes the magnetic data for both compounds.

Finally, the magnetic properties of both compounds may be explained from structural data, by assuming that the ferromagnetic behavior is mainly due to intradimer coupling and the antiferromagnetic arrangement at low temperature to interdimer interactions. Specific heat measurements

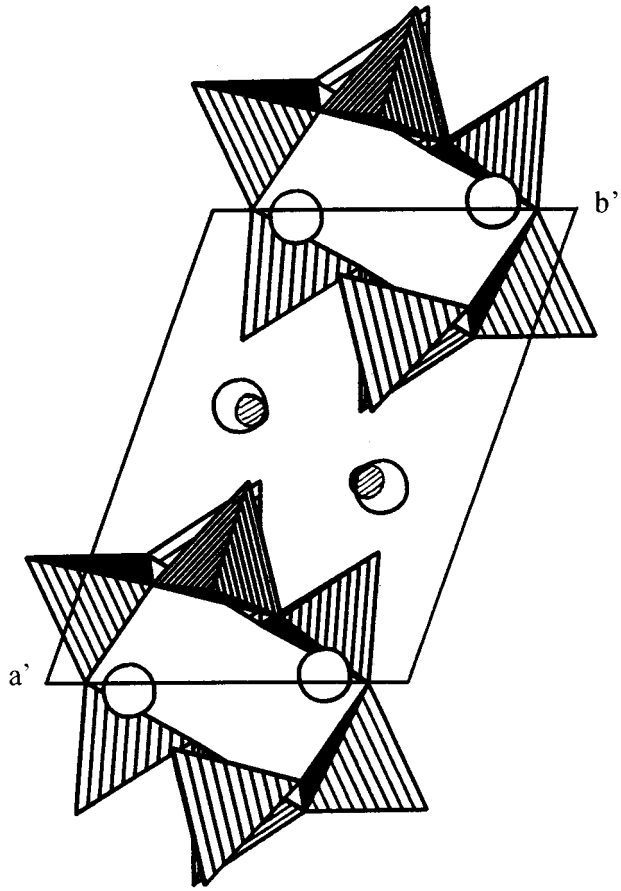


**FIG. 2.** Projection of the $Na_2MSi_4O_{10}$ structure on the $a'b'$ plane showing the $(Si_8O_{20})^{8-}$ units. The $a'b'c'$ unit cell results from a conversion of the unit cell reported in Table 1 using the matrix (111/011/001) (2). The open and shaded circles correspond to Na and $M$ atoms, respectively.

have been performed at low temperatures to detect the occurrence of a long-range ordering.

*Specific Heat Measurements*

The temperature dependence of the specific heat shows, for both compounds, the presence of a Schottky-type anomaly with a maximum in the range 3–5 K. This anomaly is important for the cobalt(II) compound and less pronounced for the nickel(II) derivative. From the relationship $Cp = aT^{-2} + bT^3$, where the first term is related to magnetic correlations and the second to lattice contribution, we deduce the specific heat of magnetic origin (Fig. 7) (7). Clearly, the observed variation of Cp confirms that short-range correlations dominate the magnetic behavior in the temperature range of interest. The stabilization of a magnetic ground state for dinuclear units does not promote (for $T > 1.5$ K) a long-range order.

**TABLE 4**
**Comparison of Interatomic Distances (Å) for $M$ = Cu, Co, Ni**

| | Cu | Co | Ni |
|---|---|---|---|
| | | *M*–O | |
| CN | 4 + 1 | 5 | 5 |
| Base | 1.967 | 2.01 | 2.06 |
| Apex | 2.511 | 2.14 | 2.14 |
| | | *M*–*M* | |
| Intradimer | 3.357 | 3.23 | 3.17 |
| Interdimer | 5.003–5.791 | 5.30–5.69 | 5.24–5.71 |
| | | Si–O | |
| Average | 1.607 | 1.63 | 1.61 |
| Nonbridging | 1.571 | 1.58 | 1.55 |
| Bridging | 1.631 | 1.64 | 1.63 |
| | | Na(1)–O | |
| CN | 7 | 7 | 7 |
| Average | 2.554 | 2.60 | 2.60 |
| | | Na(2)–O | |
| CN | 6 + 1 | 6 + 1 | 6 + 1 |
| Average (7) | 2.590 | 2.64 | 2.62 |
| Average (6) | 2.514 | 2.55 | 2.54 |

*Magnetic Behavior Modelization*

Since no $\lambda$-type anomaly was detected on the specific heat curve, a fitting of the $\chi T = f(T)$ curve for the nickel compound (continuous line in Fig. 6) has been performed to get

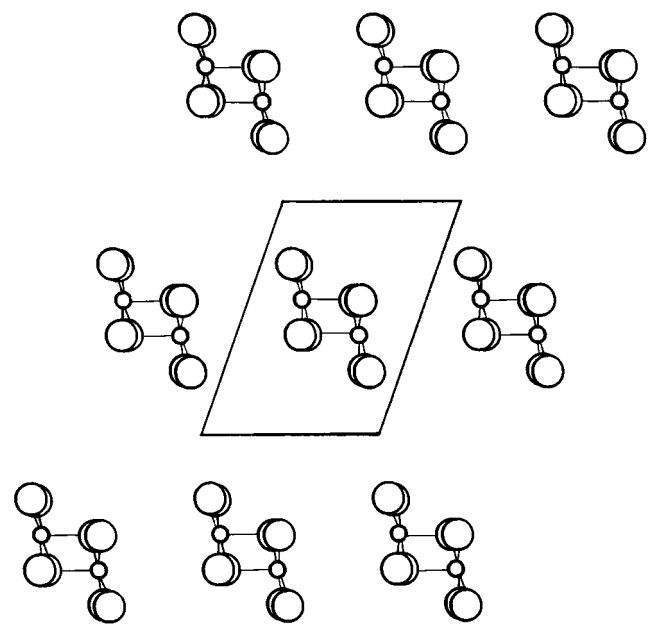

**FIG. 3.** $(M_2O_8)^{4-}$ dimers projected on the $a'b'$ plane.

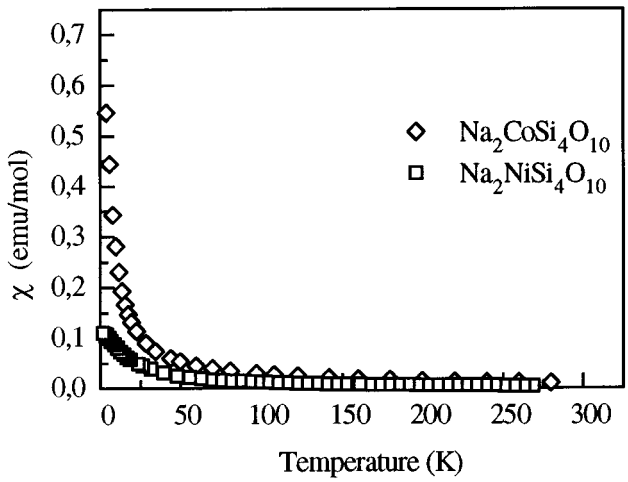


**FIG. 4.** Magnetic susceptibility ($\chi$) evolutions versus temperature for $Na_2MSi_4O_{10}$.

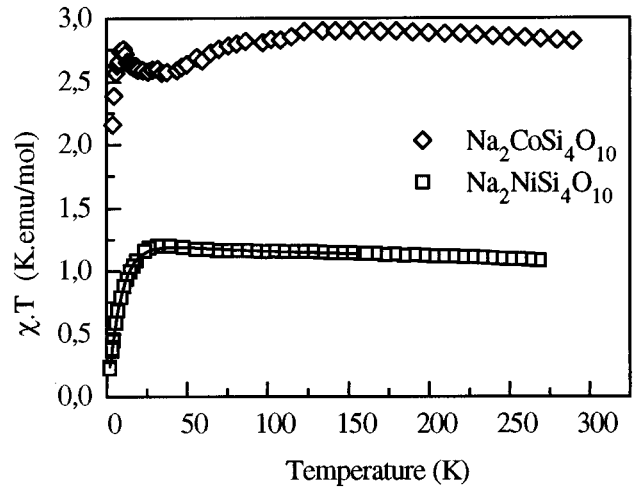


**FIG. 6.** $\chi T$ product evolutions versus temperature for $Na_2MSi_4O_{10}$. The continuous line for Ni sample represents the fitted $\chi T = f(T)$ curve.

more insight in the magnetic behavior. The expression of the magnetic susceptibility has been deduced from the spin Hamiltonian

$$H = -2JS_1S_2 - D(S_{1z}^2 + S_{2z}^2) - g\mu_B H(S_{1z} + S_{2z}) - 2zjS_z\langle S\rangle,$$

$J$ and $j$ refering to intra- and interdimer interactions, respectively, and $D$ being the anisotropy parameter. The best fit was obtained with the parameters $J = 10.9$ K, $j = -1.9$ K, $D = -16$ K, and $g = 2.09$. Both $g$ and $J$ determine the $\chi T$ evolution at temperature higher than 50 K whereas $D$ and $j$ are more influential at lower temperature. These results clearly confirm the proposed mechanism with ferromagnetic intradimer interactions and antiferromagnetic interdimer interactions. Moreover, it is not so surprising that the maxima observed on Cp are located under 10 K, due to the existence of these antiferromagnetic interdimer interactions. Therefore, these latter imply a decrease in the Schottky anomaly temperature below 5 K. The fact that no $\lambda$-type anomaly is observed means that no long-range order is established at the lowest measured temperature. Order could therefore take place at lower temperature.

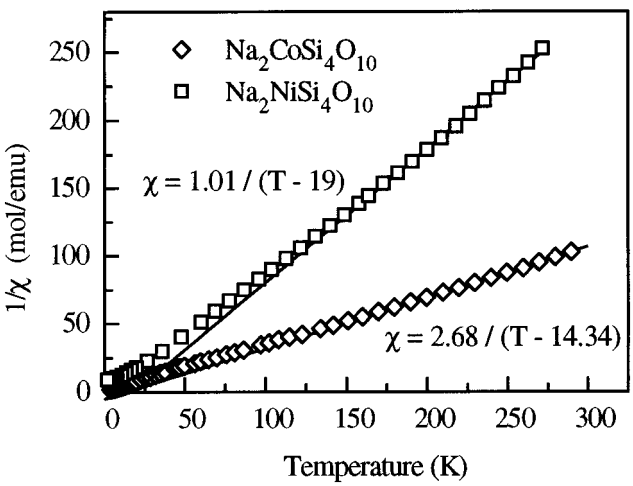


**FIG. 5.** Inverse magnetic susceptibility ($1/\chi$) evolutions versus temperature for $Na_2MSi_4O_{10}$.

## SUMMARY

$Na_2MSi_4O_{10}$ compounds ($M$ = Co, Ni) have been prepared by calcination at 700°C of a mixture obtained from Na and Si alkoxides and $M$ nitrate. Crystallization proceeds progressively with intermediate formation of a mixture containing $M$ oxide, $Na_2MSi_4O_{10}$, and an unidentified phase, and no exotherm was detected on the corresponding DTA traces. Co and Ni samples appear to be isostructural with the corresponding Cu compound. The main difference with the copper phase concerns the environment of the transition metal: whereas Co and Ni have a quite regular oxygen square pyramid around them, a strong axial deformation was observed for Cu (2). The magnetic behaviors agree with the structural findings: ferromagnetic interactions are observed within the $(M_2O_8)^{4-}$ units, while antiferromagnetic interdimer interactions dominate at low temperature.

**TABLE 5**
**Magnetic Data of $Na_2MSi_4O_{10}$ Compounds**

| $M$ | $\chi T$ max(K) | $C$ (emu K/mol) | $\theta$ (K) |
|---|---|---|---|
| Ni | 35 | 1.01 | 19.0 |
| Co | 10 | 2.68 | 14.3 |

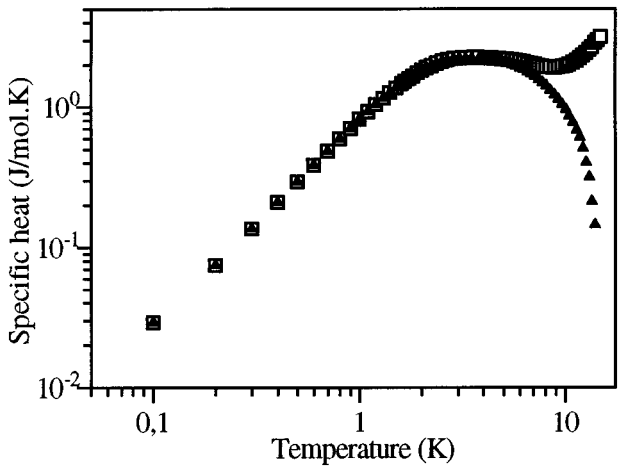


**FIG. 7.** Specific heat evolution versus temperature (in a log–log representation) for $Na_2CoSi_4O_{10}$. The squares represent the experimental points, and the triangles the calculated specific heat of magnetic origin.

## REFERENCES

1. G. Durand, S. Vilminot, P. Rabu, A. Derory, J. P. Lambour, and E. Ressouche, *J. Solid State Chem.* **124,** 374 (1996).
2. K. Kawamura and A. Kawahara, *Acta Crystallogr. B* **33,** 1071 (1977).
3. J. Rodriguez-Carvajal, "Fullprof Program, Version 2.4.2." I.L.L., Grenoble, December 1993. [Original code provided by D. B. Wiles, R. A. Young, and A. Sakthivel]
4. The calorimeter was designed by R. Kuentzler and Y. Dossmann (Strasbourg) for measurements in the temperature range 0.9–40 K. It is made of an adiabatic chamber with a saphire sample holder, equipped with a Ge resistance thermometer and an evaporation deposit Cr/Ti heater. The sample holder is suspended with nylon threads. The accuracy of the measurements is better than 1%.
5. Y. Hubert, J. L. Guth, B. Perati, and R. Wey, *C. R. Acad. Sci. Paris* **283,** 291 (1976).
6. Y. Hubert, D. Jordan, J. L. Guth, and A. Kalt, *C. R. Acad. Sci. Paris* **284,** 329 (1977).
7. R. L. Carlin, "Magnetochemistry," p. 165. Springer-Verlag, Berlin, Heidelberg, 1986.